VII International Conference on Computational Methods in Marine Engineering
MARINE 2017
M. Visonneau, P. Queutey and D. Le Touzé (Eds)

ON THE NUMERICAL CONVERGENCE PROPERTIES OF THE CALCULATION OF THE FLOW AROUND THE KVLCC2 TANKER IN UNSTRUCTURED GRIDS

Ana Luísa Rocha*, Luís Eça* and Guilherme Vaz†

*Instituto Superior Técnico
Universidade de Lisboa
Av. Rovisco Pais, 1049-001 Lisboa, Portugal
e-mail: ana.luisa.rocha@tecnico.ulisboa.pt
e-mail luis.eca@tecnico.ulisboa.pt

† Maritime Research Institute Netherlands (MARIN)
2, Haagsteeg
6708 PM Wageningen, The Netherlands
e-mail: G.Vaz@marin.nl

Key words: RANS, Numerical Error, Unstructured Grids, KVLCC2

Abstract. This paper addresses the estimation of numerical errors in the calculation of the flow around the KVLCC2 tanker at model scale Reynolds number in unstructured grids. The flow solution is based on the Reynolds-Averaged Navier-Stokes equations supplemented by the $k-\omega$ SST two-equation eddy-viscosity model using the so-called double-body approach, i.e. free surface effects are neglected. Grid refinement studies are performed for sets of grids generated with the open source code SnappyHexMesh and with the HEXPRESS^{TM} grid generator. Definition of grid refinement ratio in unstructured grids and its consequences for the estimation of numerical errors is discussed. Friction and pressure resistance coefficients and mean velocity components at the propeller plane are compared with reference solutions obtained in nearly-orthogonal multi-block structured grids with the same flow solver ReFRESCO.

1 INTRODUCTION

Calculation of viscous flows around ships at model and full scale Reynolds numbers based on the Reynolds-Averaged Navier-Stokes equations has become standard practice for many CFD flow solvers. The two main challenges that such calculations present are: the ability to reduce the numerical error (iterative and discretization errors) to negligible levels and the selection of the turbulence model that leads to the smallest modelling errors. Recently, a Verification and Validation study has been performed for the KVLCC2 tanker [1] which is a ship geometry that has been thoroughly studied since the 2000 Gothenburg Workshop [2].

In [1], thirteen different turbulence models including one-equation and two-equation eddy-viscosity models and Explicit Algebraic Reynolds Stress Models are tested neglecting free surface

effects and applying no-slip conditions without wall functions. Discretization errors are estimated with grid refinement studies [4] using sets of nearly-orthogonal multi-block structured grids generated with GridPro [3]. In all the simulations presented in [1], it was possible to reduce the iterative error[1] to negligible levels when compared to the discretization error. However, as the geometric complexity of the ship increases, as for example with the use of an energy saving device in the JAPAN Bulk Carrier proposed for the 2015 Tokyo Workshop [5], there is a natural trend to use unstructured grids [6].

Generation of unstructured grids has significantly progressed in the last two decades with several open-source and commercial codes available. There are (at least) two common features in most of the viscous flow simulations performed in unstructured grids: the use of near-wall layers of cells that intend to preserve grid orthogonality in the near-wall region and the use of local refinement boxes. This latter feature can originate the so-called hanging nodes that may affect the iterative and discretization errors of the numerical solutions. Therefore, it is important to investigate the impact of the use of unstructured grids on the numerical accuracy of ship viscous flows. To this end, we have selected the flow around the KVLCC2 tanker[2] at model scale Reynolds number with the same domain size and boundary conditions used in the study presented in [1]. Our goal is twofold: address iterative and discretization errors of RANS solutions performed in unstructured grids generated with two different grid generators: an open source code SnappyHexMesh [7] and the commercial package HEXPRESS$^{\text{TM}}$ [8]; investigate the use of grid refinement studies and power series expansions to estimate discretization errors for unstructured grids.

Although the results presented in [1] show that discretization errors for a given grid depend on the selected turbulence model and quantity of interest, in the present exercise, we have restricted ourselves to the shear-stress transport (SST) $k-\omega$ two-equation eddy-viscosity model [9]. Furthermore, the quantities of interest selected for this study are only the friction and pressure resistance coefficients and the mean flow axial velocity component at the locations of the propeller plane that have experimental measurements available [10].

It must be mentioned that generating grids with SnappyHexMesh for the calculation of the flow around the KVLCC2 tanker without wall functions is not a trivial task, even for model scale Reynolds number. Although we can not guarantee that it is impossible to keep the dimensionless near-wall cell height below 1 ($y^+_{nw} < 1$), all the attempts made were unsuccessful. Furthermore, it is not easy to keep y^+_{nw} above 50 for the complete surface of the ship and so calculations for grids generated with SnappyHexMesh had to be performed with the so-called Automatic Wall Functions, which blend the linear sub-layer with the log-law region [11]. Therefore, we have generated two sets of grids[3] with HEXPRESS$^{\text{TM}}$: one with a near-wall cell size similar to the SnappyHexMesh grids and a second set with $(y^+_{nw})_{max} < 1$. The first set of grids provides a comparison to the SnappyHexMesh results, whereas the second set is compared to the results presented in [1] for the same problem and flow solver ReFRESCO [12].

The paper is organized in the following way: section 2 presents the problem definition, whereas section 3 presents the sets of unstructured grids used in this study and the determination of the

[1]Iterative convergence required maximum normalized residuals of all transport equations solved below 10^{-8}. Residuals of transport equations are equivalent to changes of dimensionless variables in a simple Jacobi iteration.

[2]Defined by the same stl file used in [1].

[3]The original plan was to use only open source codes.

grid refinement ratio (typical cell size); the results are presented and discussed in section 4 and the conclusions are summarized in section 5.

2 PROBLEM DEFINITION

2.1 Mathematical Model

In the present work we have adopted the time-averaged continuity and Navier-Stokes (RANS) equations for an incompressible fluid $\rho = const.$ supplemented with the SST two-equation $k-\omega$ eddy-viscosity model described in [9, 13]. It should be mentioned that the production term of the k transport equation is limited to 15 times dissipation k ($\varepsilon = \beta^* k\omega$), which is slightly different from the 10 times ε suggested in [9]. However, the purpose of this limiter is to avoid an unphysical overshoot of ν_t at the stagnation region and tests performed for a flat plate flow [14] show that the limiter with 10 times ε is also active in several regions of the boundary-layer.

2.2 Calculation Domain

The domain for the calculation of the flow around the KVLCC2 tanker at model scale Reynolds number is exactly equal to that adopted in [1]. It is a prismatic rectangular region defined in a Cartesian coordinate system[4] (x, y, z) with the x axis coincident with the keel line (pointing to the bow), the transverse y axis perpendicular to the symmetry plane of the ship and the vertical z axis forming a right-handed system. The calculation domain is illustrated in figure 1.

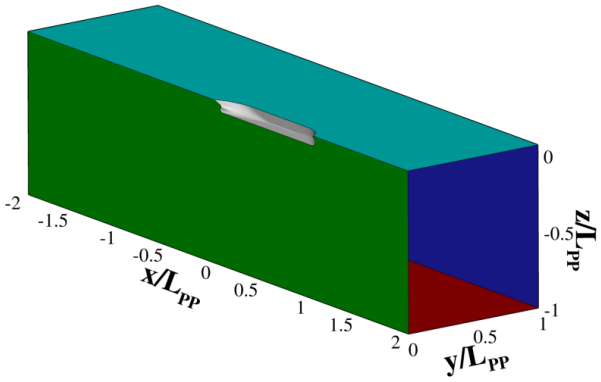

Figure 1: Illustration of the calculation domain of the flow around the KVLCC2 tanker.

The Reynolds number Re based on the incoming flow velocity V_∞ and the distance between perpendiculars L_{PP} is equal to

$$Re = \frac{V_\infty L_{PP}}{\nu} = 4.6 \times 10^6 \ .$$

It must be mentioned that the KVLCC2 surface definition is based on the same stl file used in [1], which includes a fairing of the transom of the stern. This small change of the original

[4]The origin of the coordinate system is on the symmetry plane of the ship at the intersection of the keel line and aft perpendicular.

geometry avoids iterative convergence problems due to detached flow separation regions and the occurrence of vortex shedding.

2.3 Boundary Conditions

The computational domain is bounded by the following surfaces: the surface of the ship and its symmetry plane ($y = 0$); the still water[5] plane located at $z = 0.065L_{PP}$; the inlet and outlet planes located at $x = \pm 2L_{PP}$; the lateral plane located at $y = L_{PP}$ and the bottom plane placed at $z = -L_{PP}$.

Velocity components are set equal to undisturbed flow conditions at the inlet, $x = 2L_{PP}$, i.e. $V_x = V_\infty$, $V_y = 0$ and $V_z = 0$ and the pressure is extrapolated from the interior of the domain. Turbulence kinetic energy is specified from a turbulence intensity of $I = 1\%$ and the ω value is specified to obtain $\nu_t = 0.1\nu$. Streamwise derivatives of all dependent variables are assumed to be zero at the outlet $x = -2L_{PP}$. Symmetry conditions are applied at the still water plane ($z = 0.065L_{PP}$) and at the symmetry plane of the ship, whereas free slip conditions are applied at the bottom boundary $z = -L_{PP}$. Pressure is fixed at the lateral boundary ($y = L_{PP}$) and transverse velocity derivatives of the remaining dependent variables are assumed to be zero.

At the ship surface, velocity components are set equal to zero due to impermeability and the no-slip condition and the pressure derivative in the normal direction to the surface is set equal to zero. k is set equal to zero at the ship surface and ω is specified at the near-wall cell centre using the blend of the linear sub-layer and log-law regions proposed in [11]. The determination of the shear-stress at the wall τ_w depends on the height of the near-wall cells, i.e. on y^+_{nw}. For the HEXPRESS$^{\text{TM}}$ grids (see section 3.2) with $y^+_{nw} < 1$, τ_w is determined directly from its definition, whereas for all the other grids used in this study the velocity profile proposed in [11] is used to determine τ_w and the production of k in the near-wall cell is based on τ_w.

3 GRID GENERATION

The original goal of this study was to generate unstructured grids using only the open source grid generator SnappyHexMesh [7]. However, a mandatory condition was to be able to generate grids suitable for the application of the no-slip condition without the use of wall functions. Unfortunately, we have not succeeded in fulfilling this requirement with SnappyHexMesh and so we have also used the commercial grid generator HEXPRESS$^{\text{TM}}$ to generate sets of unstructured grids that exhibit $y^+_{nw} < 1$. On the other hand, results obtained in the SnappyHexMesh grid sets cannot be directly compared with the results given in [1] due to the change in the calculation of the shear-stress at the wall (with or without wall functions). Therefore, we have generated a second grid set with HEXPRESS$^{\text{TM}}$ that presents similar values of y^+_{nw} to those obtained in the SnappyHexMesh grids.

3.1 SnappyHexMesh Grids

SnappyHexMesh is an unstructured grid generator that is included in the open source CFD software OpenFOAM [7]. The grid generation process in the SnappyHexMesh utility is done in three consecutive steps: creation of an hexahedral parametric grid covering the whole domain

[5] Free surface effects are neglected.

without the ship surface using the BlockMesh utility; introduction of the ship geometry defined with a triangulated surface geometry file in Stereolithography (STL) format; insertion of near-wall cell layers that provide the required near-wall cell height for the application of the no-slip condition.

The most delicate step of the procedure is the latter. There are several utilities for layer refinement within OpenFOAM [7]. However, we have used SnappyHexMesh for both layer addition and refinement, because all other alternatives lead to unacceptable cells (negative Jacobian), especially at the stern of the ship.

The grid generation procedure adopted tried to keep geometrical similarity of the grids as much as possible. To this end, the twelve different blocks defined in BlockMesh (step 1) were systematically refined in the x, y and z directions to create a set of eight basis grids. In the second step of the procedure that iteratively conforms the grid to the 3-D geometry of the KVLCC2 hull, we have adopted two different approaches: for grid set S1 a single refinement box with an extra refinement level of three is set around the whole hull; extra refinement boxes were added at the bow and stern of the ship for grid set S2. As mentioned above, none of the strategies tested enabled the generation of grids with $y^+_{nw} < 1$ using the tools available in the OpenFoam [7] toolbox. Therefore, we generated grids appropriate for the application of the no-slip condition with wall functions, i.e. $y^+_{nw} > 30 - 50$. This was accomplished for the eight grids of sets S1 and S2 using a trial and error approach. As a consequence, the two grid sets present two main difficulties: the insertion of near-wall cell layers must be tuned grid by grid and so geometrically similarity is naturally destroyed; it is not possible to keep $y^+_{nw} > 30 - 50$ for the complete ship surface and so "automatic" wall functions [11] must be used for the application of the no-slip condition.

Table 1: Number of interior cells N_c , number of cells on the ship surface N_s and average $(y^+_{nw})_{\text{avg}}$, maximum $(y^+_{nw})_{\max}$ and minimum $(y^+_{nw})_{\min}$ values of the dimensionless near-wall cell height of the eight grids of sets S1 and S2 generated with SnappyHexMesh.

	N_c	N_s	y^+_{nw}				N_c	N_s	y^+_{nw}		
	$\times 10^{-6}$	$\times 10^{-5}$	avg	max	min		$\times 10^{-6}$	$\times 10^{-5}$	avg	max	min
$S1_1$	22.2	5.52	45.3	72.5	0.98	$S2_1$	21.8	3.35	40.1	69.1	0.29
$S1_2$	15.8	4.36	45.2	72.2	1.00	$S2_2$	15.6	2.65	36.4	78.6	0.18
$S1_3$	11.1	3.34	46.0	110.	1.65	$S2_3$	10.8	2.03	37.1	88.8	0.11
$S1_4$	7.12	2.46	46.0	72.6	1.58	$S2_4$	6.91	1.49	35.7	93.2	0.34
$S1_5$	4.48	1.71	46.0	129.	2.19	$S2_5$	4.11	1.03	40.7	81.8	0.38
$S1_6$	2.62	1.09	47.4	188.	1.20	$S2_6$	2.21	0.67	37.0	112.	0.40
$S1_7$	1.30	0.62	46.3	254.	3.41	$S2_7$	1.05	0.37	42.1	211.	0.69
$S1_8$	0.86	0.42	49.3	428.	1.04	$S2_8$	0.63	0.26	41.8	190.	0.58

Table 1 presents the number of interior cells N_c, the number of cells on the ship surface N_s and the average $(y^+_{nw})_{\text{avg}}$, maximum $(y^+_{nw})_{\max}$ and minimum $(y^+_{nw})_{\min}$ values of the dimensionless near-wall cell height of the eight grids of sets S1 and S2. Figure 2 presents an illustration of

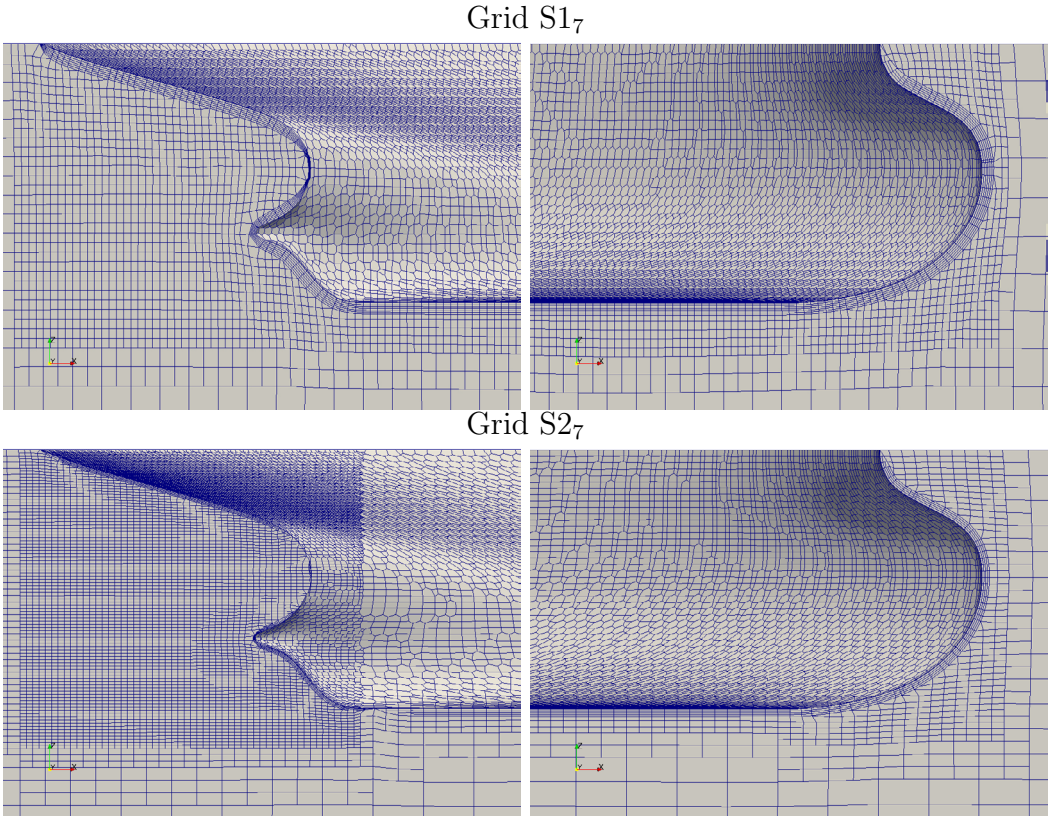

Figure 2: Illustration of the grids generated with SnappyHexMesh at the bow and stern of the KVLCC2 tanker.

grids S1$_7$ and S2$_7$ at the bow and stern regions, where it is visible the poor definition of the ship's geometry at the stern. On the other hand, the lack of control over the introduction of the near-wall cell layers is exemplified by the oscillations obtained for $(y^+_{nw})_{\text{avg}}$, $(y^+_{nw})_{\text{max}}$ and $(y^+_{nw})_{\text{min}}$. Naturally, the properties of the grids included in these two sets are far from ideal. Nonetheless, they will serve two goals on the present study: investigate the robustness of the flow solver and the estimation of discretization of errors based on power series expansions.

3.2 HEXPRESS$^{\text{TM}}$ Grids

The goal of the HEXPRESS^{TM} grid sets in this work is to generate solutions to compare with the results obtained in the SnappyHexMesh sets presented in the previous section and to the results presented in [1] obtained in multi-block structured grids.

HEXPRESS$^{\text{TM}}$ generates non-conformal body-fitted hexahedral unstructured grids on arbitrary geometries following a sequence of eight main steps. The present grids were generated with the procedure described in [15] with the hull geometry divided into seven different parts (the bulbous bow, the fore-ship, the bilge, the upper-mid-ship, the lower-mid-ship, the aft-ship and the stern) in order to facilitate the surface refinements and the posterior addition of the prismatic layers.

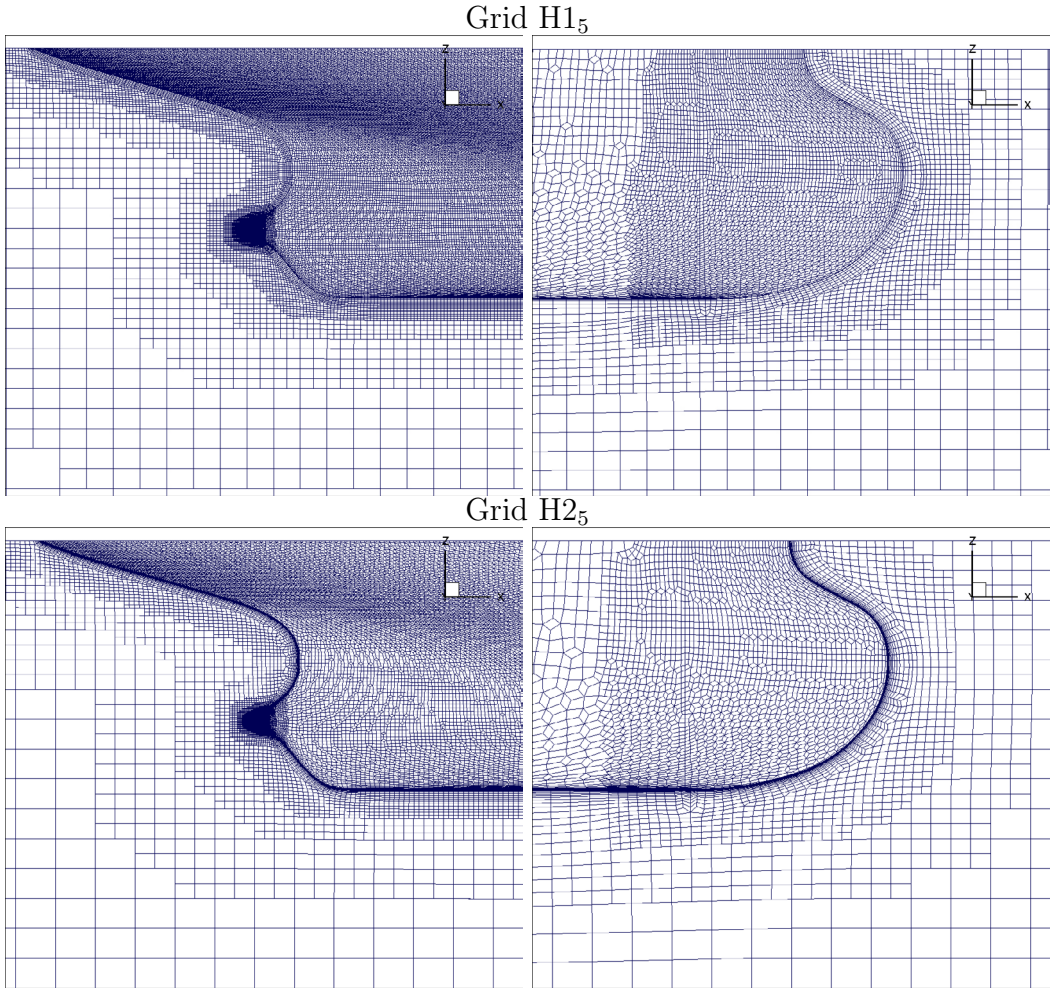

Figure 3: Illustration of the grids generated with HEXPRESS$^{\text{TM}}$ at the bow and stern of the KVLCC2 tanker.

Two sets of six grids were generated with HEXPRESS$^{\text{TM}}$: set H1 includes grids with $(y^+_{nw})_{\text{avg}} \simeq 30 - 50$ and set H2 grids with $(y^+_{nw})_{\text{max}} < 1$. Compared to the grids used in [15], the present grids include extra grid refinement in the near-wake region. Table 2 presents N_c, N_s, $(y^+_{nw})_{\text{avg}}$, $(y^+_{nw})_{\text{max}}$ and $(y^+_{nw})_{\text{min}}$ of the six grids of sets H1 and H2 and figure 3 presents an illustration of grids H1$_5$ and H2$_5$ at the bow and stern regions. As expected, the control over the insertion of the near-wall cell layers is significantly better than in SnappyHexMesh.

3.3 Definition of Grid Refinement Ratio r_i

The use of power series expansions to estimate the discretization error of numerical solutions requires the definition of the typical cell size h_i to define the grid refinement ratio $r_i = h_i/h_1$, where h_1 stands for the typical cell size of the finest grid [4]. In sets of unstructured grids, it is not possible to keep strict geometrical similarity and so it is important to check the influence of

Table 2: Number of interior cells N_c , number of cells on the ship surface N_s and average $(y^+_{nw})_{\text{avg}}$, maximum $(y^+_{nw})_{\max}$ and minimum $(y^+_{nw})_{\min}$ values of the dimensionless near-wall cell height of the six grids of sets H1 and H2 generated with HEXPRESS$^{\text{TM}}$.

	N_c	N_s	y^+_{nw}				N_c	N_s	y^+_{nw}		
	$\times 10^{-6}$	$\times 10^{-5}$	avg	max	min		$\times 10^{-6}$	$\times 10^{-5}$	avg	max	min
$H1_1$	23.3	9.71	32.4	56.8	0.02	$H2_1$	24.0	3.58	0.06	0.10	0.002
$H1_2$	13.7	6.27	33.6	62.7	0.04	$H2_2$	14.5	2.51	0.08	0.12	0.001
$H1_3$	7.09	3.58	39.7	66.1	0.13	$H2_3$	7.84	1.62	0.09	0.15	0.005
$H1_4$	2.94	1.64	42.6	70.5	0.18	$H2_4$	3.61	0.92	0.13	0.19	0.004
$H1_5$	1.49	0.94	43.9	71.8	0.37	$H2_5$	1.36	0.43	0.19	0.28	0.005
$H1_6$	0.61	0.43	45.3	73.1	0.22	$H2_6$	0.30	0.13	0.36	0.53	0.026

the r_i definition on the estimated uncertainties. In this study, we have determined r_i based on the volume of the grid cells V and on the area of the ship surface cells S using $r_i = (V_i/V_1)^{1/3}$ or $r_i = (S_i/S_1)^{1/2}$.

For a grid with N_c interior cells and N_s cells on the ship surface, four different values of V and S are determined:

1. The mean value of the cells volume V^1 and area S^1,

$$V^1 = \frac{\sum_{j=1}^{N_c} V_j}{N_c} \quad \text{and} \quad S^1 = \frac{\sum_{j=1}^{N_s} S_j}{N_s} \, .$$

2. The root mean squared value of the cells volume V^2 and area S^2,

$$V^2 = \sqrt{\frac{\sum_{j=1}^{N_c} V_j^2}{N_c}} \quad \text{and} \quad S^2 = \sqrt{\frac{\sum_{j=1}^{N_s} S_j^2}{N_s}} \, .$$

3. The mode of the cells volume V^m and area S^m, which corresponds to the values of V and S that occur more often. V^m and S^m are determined from an histogram containing forty intervals of constant width in logarithm scales. The values of V^m and S^m are equal to the mid-point of the interval containing the largest number of cells.

4. The maximum value of the cells volume V^M and area S^M, $V^M = \text{MAX}\,(V_j)$ and $S^M = \text{MAX}\,(S_j)$.

If the grids of a given set were strictly geometrically similar, the values of r_i based on V^1, V^2, V^m, V^M, S^1, S^2, S^m and S^M would be all equal. In the present grid sets, the values of r_i obtained from the eight alternatives described above are not identical, as illustrated in figure 4.

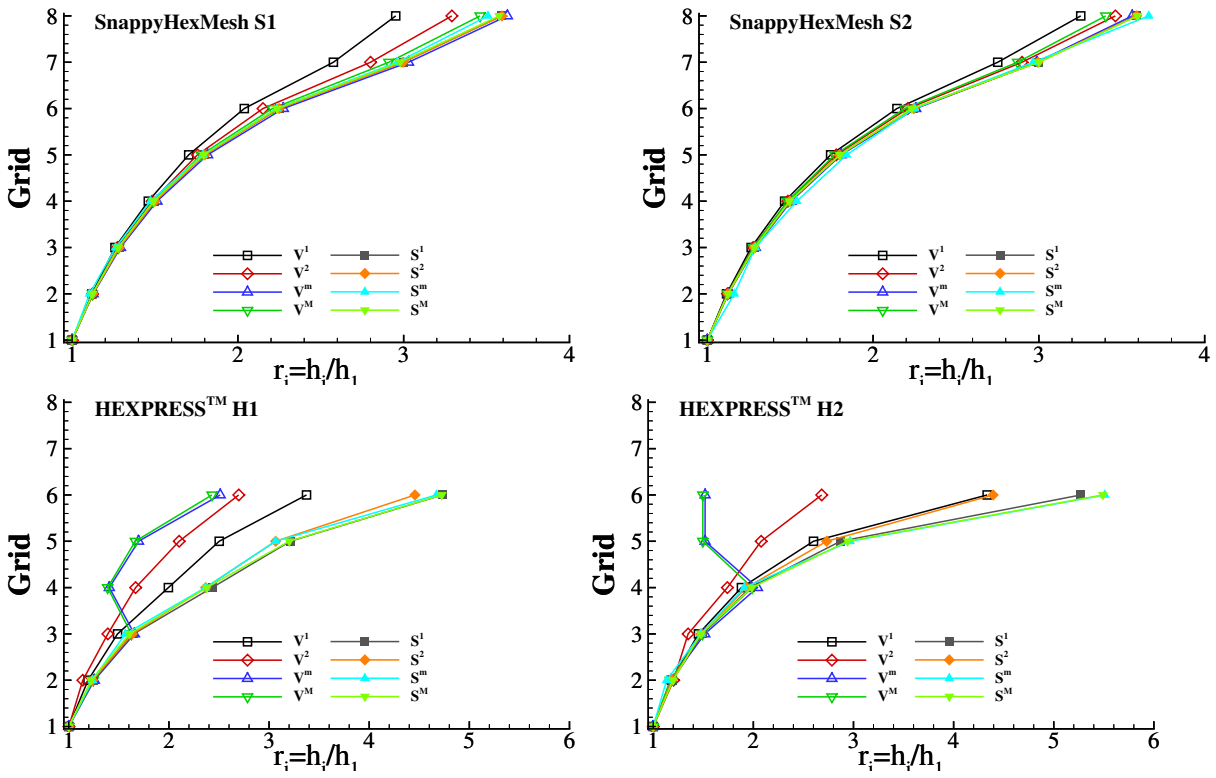

Figure 4: Grid refinement ratio r_i obtained from the mean (^{1}), root mean squared (^{2}), mode (^{m}) and maximum (^{M}) volume of the interior cells (V) and area of the ship surface cells (S).

Although there are significant differences between the results obtained for the SnappyHexMesh and HEXPRESS$^{\text{TM}}$ grid sets, there are two common trends in the four grid sets: for a given set, the grids on the ship surface are nearly geometrically similar due to the resemblance of all values based on S; the differences between the different values of r_i increase with the grid coarsening.

For the S1 and S2 sets, the two alternatives based on V that lead to the results most similar to those obtained with S are V^m and V^M. However, these two alternatives are completely unreliable for the H1 and H2 sets due to the changes in grid topology obtained for the coarsest grids of these sets in the outer parts of the domain. As illustrated in figure 5 for the four coarsest grids of set H2, the largest cells reduce size from $H2_4$ to $H2_5$ and remain almost identical between $H2_5$ and $H2_6$. A similar phenomena occurs for the coarsest grids of the H1 set. Therefore, defining r_i based on S seems to be a better choice than using V. Nonetheless, we will compare the estimation of discretization errors using these eight definitions of r_i. Naturally, we drop the values of r_i obtained from V^m and V^M for grid sets H1 and H2.

4 RESULTS

4.1 Numerical Details

The calculations performed for the S1, S2, H1 and H2 grid sets were performed with a segregated approach and the diffusion terms of all transport equations approximated by second-

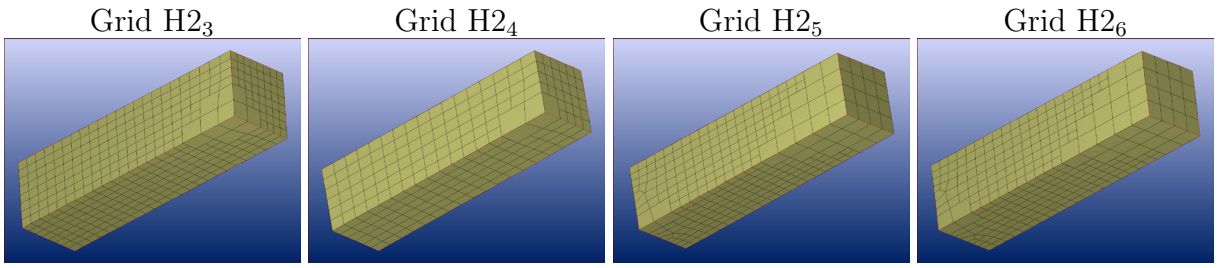

Figure 5: Illustration of the H2 grids generated with HEXPRESS^{TM} in the outer part of the domain.

order central differences including non-orthogonality corrections [16, 17]. For the S1 and S2 grids, all calculations were performed with second-order upwind (QUICK) with limiters (QL) in the convective terms of the momentum equations and first-order upwind applied to the convective terms of the k and ω transport equations. For the H1 and H2 grids two alternatives were tested: second-order upwind without limiters (Q) in the convective terms of the momentum equations; second-order upwind with limiters (QTL) in the convective terms of all transport equations.

The selected quantities of interest are the pressure C_P and friction C_F resistance coefficients and the Cartesian mean axial velocity components V_x at the 674 locations of the propeller plane $x = 0.0175L_{PP}$ with available experimental measurements [10].

4.2 Iterative Errors

The iterative convergence criteria targeted for all the present simulations was a maximum normalised residual (L_∞ norm) for all transport equations of 10^{-8}. Normalised residuals are equivalent to dimensionless variable changes in a simple Jacobi iteration with ρ, V_∞ and L_{PP} used as reference quantities. Not all the simulations were able to attain such level of iterative convergence with residuals stagnating at a higher level than desired in some cases.

Overall, iterative converge is worse for the SnappyHexMesh (S1 and S2) grids than for the HEXPRESS^{TM} (H1 and H2) grids. Only three grids of set S1 converged to the required tolerance ($S1_2$, $S1_3$ and $S1_4$) and convergence stagnated for residuals of momentum and continuity equations of the order 10^{-4} for grid $S1_6$ and 10^{-5} for the remaining grids of this set. On the other hand, the six coarsest grids of the S2 set satisfy the selected convergence criteria and the calculations in the two finest grids were stopped after 10^4 iterations with the largest residuals of the order of 10^{-6}.

Almost all calculations performed with the QL and Q settings in the H1 and H2 grids converge to the selected criteria. Typical convergence histories are illustrated in figure 6 for the coarsest (QL settings) and finest (QL, Q and QTL settings) grids of set H2. As expected, the number of iterations required to satisfy the convergence criteria increases with grid refinement and is smaller for the grids of set H1 than for those of set H2. On the other hand, very similar convergence behaviours are obtained for the QL and Q settings with the exception of the $H1_2$ grid where QL leads to stagnation of the largest residuals of the momentum equations at 10^{-4}. However, the root mean squared value of the residuals (L_2 norm) dropped to 10^{-7}. Only one of the calculations performed with QTL satisfied the selected convergence criteria (grid $H1_6$).

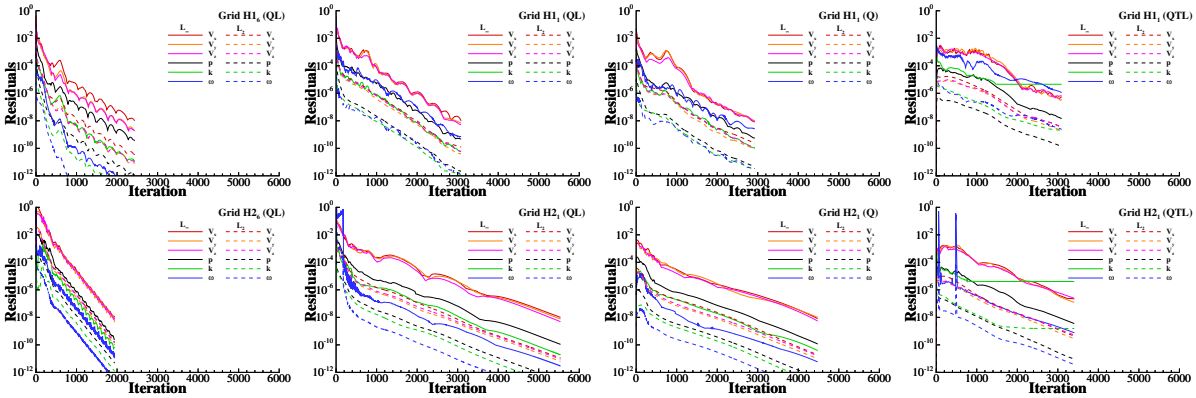

Figure 6: L_∞ and L_2 norms of the residuals of the simulations performed in the coarsest ($H1_6$ and $H2_6$) and finest ($H1_1$ and $H2_1$) grids of sets H1 and H2. Second-order upwind with (QL) and without (Q) limiters in the convective terms of the momentum equations and first-order upwind in the convective terms of the k and ω transport equations and second-order upwind with limiters in all transport equations (QTL).

However, as illustrated in figure 6, the residuals of the k transport equation stagnate (L_∞ norm of the order of 10^{-6}) but the remaining residuals keep dropping.

4.3 Discretization Errors

One of the main goals of the present exercise is to investigate the use of unstructured grids in the estimation of discretization errors with power series expansions [4]. As discussed in section 3.3, we have defined the grid refinement ratio r_i with eight different alternatives and estimated the uncertainty of the selected quantities of interest using all the values of r_i. As an example of the results obtained, figure 7 presents the friction C_F and pressure C_P resistance coefficients as a function of r_i for grid sets S1, S2, H1 and H2. Each plot presents the lines fitted to the five

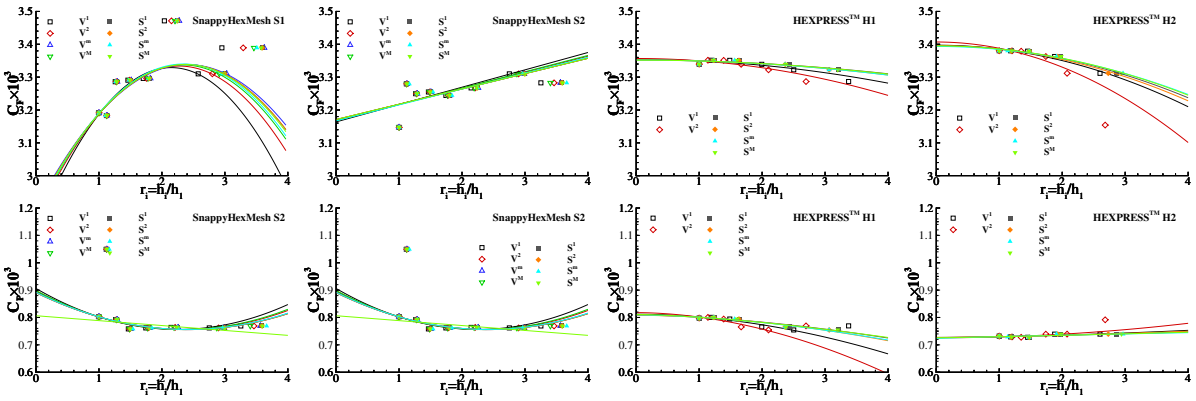

Figure 7: Convergence the friction C_F and pressure C_P resistance coefficients as a function of r_i. Second-order upwind with limiters (QL) in the convective terms of the momentum equations and first-order upwind in the convective terms of the k and ω transport equations.

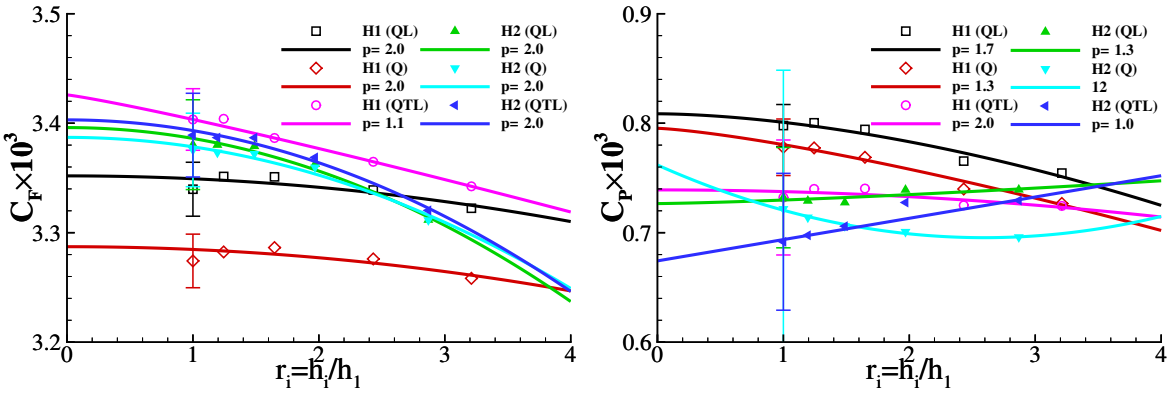

Figure 8: Convergence of the friction C_F and pressure C_P resistance coefficients as a function of r_i. Three discretization settings tested: second-order upwind with (QL) and without (Q) limiters in the convective terms of the momentum equations and first-order upwind in the convective terms of the k and ω transport equations; second-order upwind with limiters (QTL) in the convective terms of all transport equations.

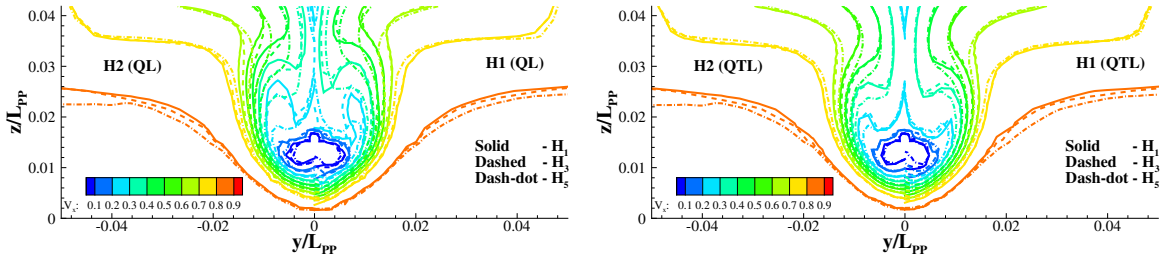

Figure 9: Isolines of mean axial velocity V_x for different levels of grid refinement. Two discretization settings: second-order upwind with limiters (QL) in the convective terms of the momentum equations and first-order upwind in the convective terms of the k and ω transport equations; second-order upwind with limiters (QTL) in the convective terms of all transport equations.

finest grids of each set with the several definitions of r_i tested.

The results obtained in the SnappyHexMesh grids exhibit a lot more scatter than the data obtained in the HEXPRESS^{TM} sets. Nonetheless, the fits performed with the several definitions of r_i tested are all very similar with just one exception for C_P in the S1 and S2 sets. This is an encouraging result for the estimation of discretization errors in sets of unstructured grids, especially for the H1 and H2 sets that exhibit minor differences in the estimated exact solutions obtained with the six definitions of r_i tested. In the remaining of the paper, we will use the values of r_i determined from the average value of the area of the cells on the ship surface S^1.

Figure 8 presents the convergence of C_F and C_P with grid refinement for the H1 and H2 grid sets using the QL, Q and QTL settings. The results show a larger influence of the discretization settings on the force coefficients with the exception of C_F on the H2 set (no wall functions). The use of second-order upwind in the turbulence model exhibits an influence on C_P that was not observed in the multi-block structured grids used in [1]. This result suggests that this

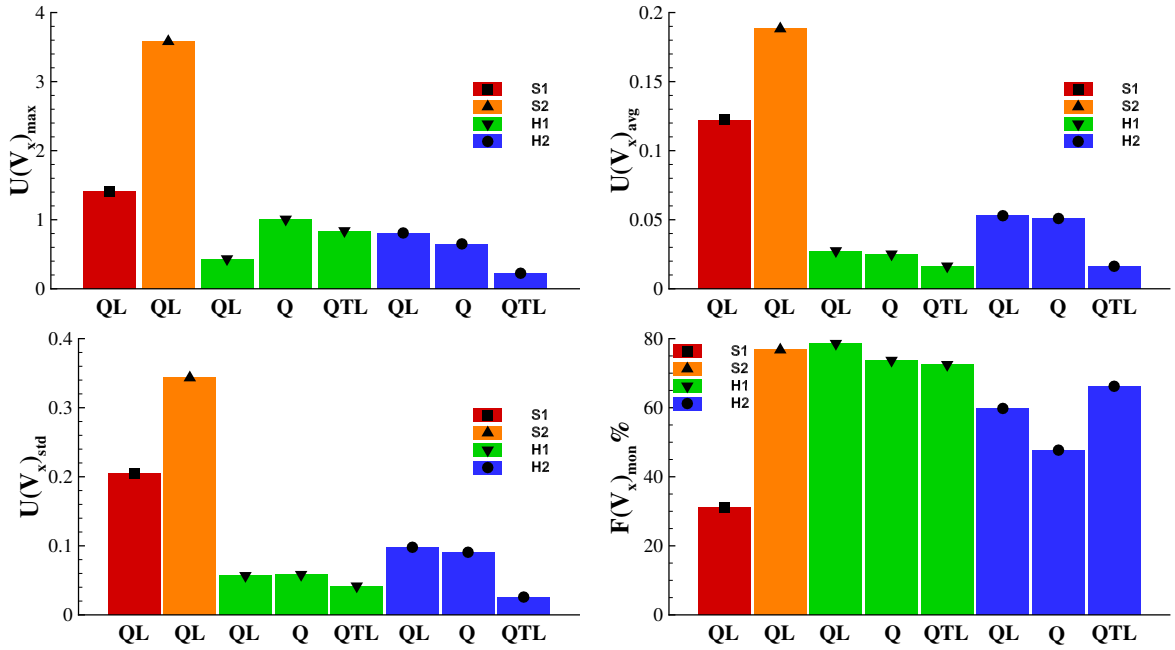

Figure 10: Maximum, average and standard deviation of the numerical uncertainty of the mean axial velocity V_x ($U(V_x)$ at the propeller plane for the finest grid of all sets. Three discretization settings: second-order upwind with (QL) and without (Q) limiters in the convective terms of the momentum equations and first-order upwind in the convective terms of the k and ω transport equations; second-order upwind with limiters (QTL) in the convective terms of all transport equations.

choice must also have a strong impact on the boundary-layer development, as illustrated by the axial velocity isolines at the propeller plane depicted in figure 9, which were obtained with the QL (left) and QTL (right) settings for three levels of grid refinement. There is a significantly larger influence of the grid size on the QL solutions than on the QTL fields, which exhibit small differences between the H_1 and H_3 grids of the two sets. Furthermore, there is a significant difference between the isolines obtained in the finest grids of the two sets with the QL and QTL settings.

Figure 10 presents the estimated numerical uncertainties of V_x at the propeller plane for all the finest grids and discretization settings presented in this paper. The plots include the maximum $U(V_x)_{\max}$, average $U(V_x)_{\text{avg}}$ and standard deviation $U(V_x)_{\text{std}}$ at the 640 locations with available experimental data and the percentage of locations that exhibit monotonic convergence $F(V_x)_{\text{mon}}$. The main trends observed in the data are: the numerical uncertainty for the SnappyHexMesh grids is significantly larger than for the HEXPRESS$^{\text{TM}}$ grids; uncertainties (and solutions) obtained with the QL and Q options are similar; the use of second-order upwind with limiters in the k and ω transport equations (QTL) reduces the numerical uncertainty of V_x, especially for the calculations performed without wall functions (H2). Therefore, we will compare both flow fields with the solutions reported in [1] in the next section.

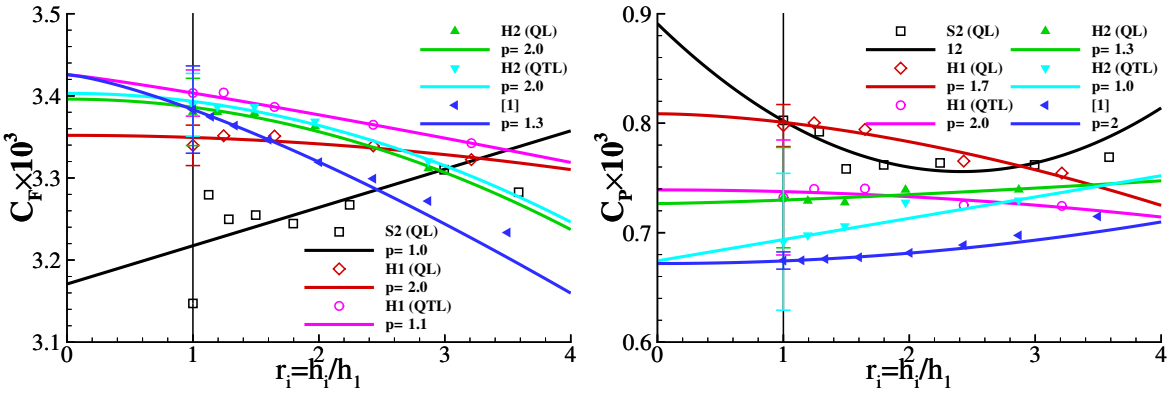

Figure 11: Convergence of the friction C_F and pressure C_P resistance coefficients as a function of r_i. Wall functions for SnappyHexMesh (S2) and HEXPRESS^{TM} (H1) and no wall functions for HEXPRESS^{TM} (H2) and the results of [1].

4.4 Comparison of Solutions

Figure 11 presents the convergence of the friction C_F and pressure C_P resistance coefficients as a function of the grid refinement for the S2(QL), H1(QL and QLT), H2(QL and QLT) solutions and the results reported in [1] for a set of multi-block structured grids. Results obtained in the S2 set exhibit a significant amount of scatter and the comparison to the results obtained in the H1 set suggest that C_F is not accurately captured in the SnappyHexMesh grids. On the other hand, the results obtained with second-order upwind in all transport equations and no wall functions H2(QTL) are in excellent agreement with the data reported in [1].

The isolines of mean axial velocity component V_x are compared in figure 12 for eight different cases: experimental data [10]; results reported in [1]; finest grids of the $S1_1$, $S2_1$, $H1_1$ and $H2_1$ sets with QL; finest grids of the $H1_1$ and $H2_1$ sets using QTL; There is (again) an excellent agreement between the $H2_1$(QTL) solution and the results reported in [1], which in this case are also similar to the $H1_1$(QTL) results. All the solutions obtained with first-order upwind in the convective terms of the k and ω transport equations (QL) exhibit V_x isolines that are closer to the experimental result than those obtained with the QTL settings. The best comparison with the experimental data is actually obtained for the $S2_1$ grid that leads to a very (numerically) innacurate prediction of the friction resistance coefficient. These results show that numerical errors may lead to a fortuitous improvement of the graphical comparison between experiments and simulations. However, if we take into account the grid sensitivity and numerical uncertainty illustrated in figures 9 and 10, it is clear that the numerical uncertainty of the results obtained with QL is not negligible. Therefore, it is important to further refine the grids of sets H1 and H2 to confirm that the results obtained with the QL settings for a sufficiently refined grid will match those obtained with second-order upwind used in the convective terms of all transport equations.

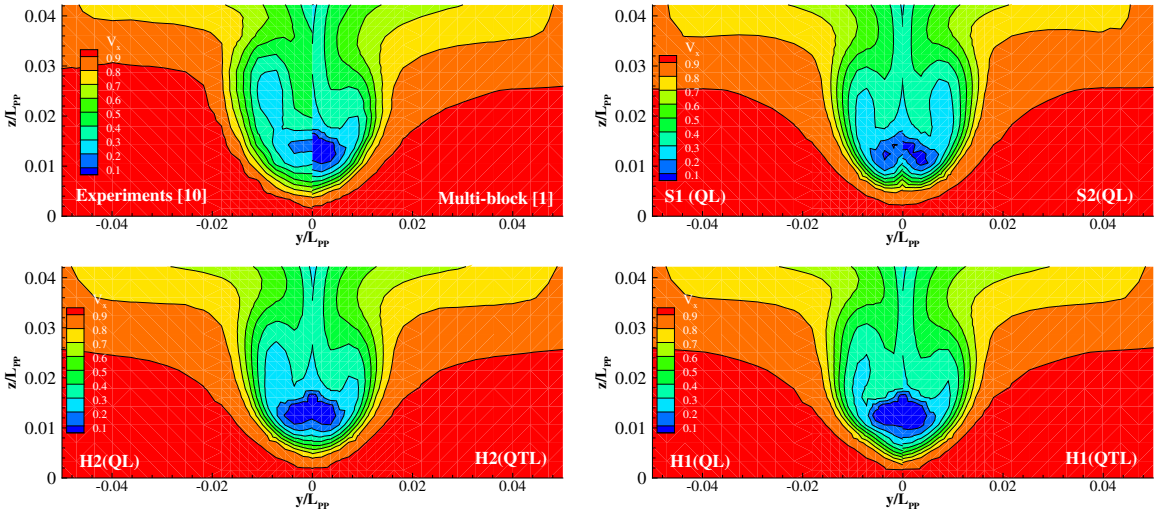

Figure 12: Isolines of mean axial velocity V_x for different levels of grid refinement. Results corresponding to experimental data [10], multi-block structured grids [1], finest grids of SnappyHexMesh sets S1 and S2 (QL) and HEXPRESS$^{\text{TM}}$ H1 and H2 (QL and QTL).

5 CONCLUSIONS

This paper addresses the estimation of discretization errors with grid refinement studies in unstructured grids. The selected test case is the flow around the KVLCC2 tanker at model scale Reynolds number, which is calculated with the Reynolds-Averaged Navier-Stokes equations supplemented with the two-equation SST $k-\omega$ eddy-viscosity model. The computational domain and selected boundary conditions are identical to those used in a similar study performed in multi-block structured grids [1].

Sets of unstructured grids were generated with the open source SnappyHexMesh program and with the commercial package HEXPRESS$^{\text{TM}}$. The generation of grids that enable the calculation of the flow around the KVLCC2 tanker without wall functions proved to be too difficult for SnappyHexMesh and so the two grid sets generated for this study require the use of the so-called "automatic" wall functions at the surface of the ship. With HEXPRESS$^{\text{TM}}$, we have generated a grid set with near-wall cells similar to those obtained with SnappyHexMesh and a second grid set that enables the calculation of the shear-stress at the wall directly from its definition, i.e. no wall functions.

Four different metrics based on the cells volume and surface area of the cells on the surface of the ship were tested to define the grid refinement ratio r_i. The results obtained for the four grid sets tested in this study suggest that the surface area of the cells on the surface of the ship is a better choice to define r_i than the cells' volume. The error estimates performed with the different ways to define r_i showed that it is possible to make reliable error estimates with power series expansions based on grid refinement studies for unstructured grids.

Calculations performed for the four grid sets showed that iterative convergence is more troublesome for the SnappyHexMesh than for the HEXPRESS$^{\text{TM}}$ grids. Therefore, the SnappyHexMesh grids calculations were all performed with first-order upwind in the convective terms

of the k and ω transport equations and second-order upwind with limiters in the convective terms of the momentum equations. On the the other hand, for the HEXPRESS$^{\text{TM}}$ grids, it is possible to converge iteratively flow fields without limiters or using second-order upwind with limiters in the turbulence quantities (k and ω) transport equations.

The results obtained for the selected quantities of interest, C_F and C_P resistance coefficients and V_x at the propeller plane, suggest the following conclusions:

- Results obtained in the SnappyHexMesh grids present a lot of scatter in the convergence with grid refinement. Comparison with HEXPRESS$^{\text{TM}}$ grids suggests that numerically accurate results require a much larger number of grid cells than the roughly 20×10^6 cells used in the finest grids of this study.

- Results obtained with first and second-order upwind in the k and ω transport equations show significant differences, with the exception of C_F for the simulations without wall functions. This trend was not observed in the grid refinement studies performed in multi-block structured grids. Furthermore, numerical uncertainty is significantly larger for the wake fields predicted with first-order upwind than for those obtained with second-order upwind in the k and ω transport equations. On the other hand, the results obtained with second-order upwind in all transport equations are in excellent agreement with data obtained for the same problem in multi-block structured grids.

- Comparison of the predicted wake fields with the experimental data is affected by error cancelling, i.e. differences between experiments and simulations diminish with the increase of the numerical error.

The results presented in this study suggest that the calculation of ship viscous flows in unstructured grids deserves to be further investigated, especially the effect of the accuracy of the discretization of the convective terms of the transport equations of the turbulence model.

Acknowledgment

The authors would like to thank P.Crepier for his help in setting up the domain and grids generated with HEXPRESS$^{\text{TM}}$.

REFERENCES

[1] Pereira F.S., Eça L. and Vaz G., *Verification and Validation Exercises for the Flow around the KVLCC2 Tanker at Model and Full-Scale Reynolds Number. Ocean Engineering*, (2017) **129**:133-148.

[2] Larsson L., Stern F. and Bertram V., *Gothenburg 2000 - A Workshop on Numerical Ship Hydrodynamics*. Chalmers University of Technology, Report CHA/NAV/R-02/0073 (2000).

[3] `www.gridpro.com`.

[4] Eça L. and Hoekstra M., *A procedure for the estimation of the numerical uncertainty of CFD calculations based on grid refinement studies. Journal of Computational Physics*, (2014) **262**:104-130.

[5] www.t2015.nmri.go.jp.

[6] Visonneau M., Deng G., Guilmineau E., Queutey P. and Wackers J., *Local and Global Assessment of the Flow around the JAPAN Bulk Carrier with and without Energy Saving Devices at Model and Full Scale*, 31st Symposium on Naval Hydrodynamics (2016) Monterey, California.

[7] Greenshields, C.J., *OpenFOAM User Guide*. http://openfoam.org, 24th June (2016).

[8] www.numeca.com/product/hexpress.

[9] Menter F.R., *Ten years of Industrial Experience with the SST turbulence model.* Turbulence Heat and Mass Transfer, (2003) **4**:625–632.

[10] Lee S. J., Kim H. R., Kim W. J. and Van S. H., *Wind Tunnel Test on Flow Characteristics of the KRISO 3,600 TEU Containership and 300K VLCC Double-Deck Ship Models.*, *Journal of Ship Research*, (2003) **47**: 24–38.

[11] Menter F.R., Esch T., *Elements of Industrial Heat Transfer Predictions.* 16th Brasilian Congress of Mechanical Engineering (2001).

[12] www.refresco.org.

[13] turbmodels.larc.nasa.gov.

[14] Eça L., *On the Limiter of the Production Term of the k Transport Equation in the SST $k-\omega$ Eddy-Viscosity Turbulence Model*, IST Report VP-8, (2008).

[15] Crepier P. *Ship Resistance Prediction: Verification and Validation Exercise on Unstructured Grids*, VII International Conference on Computational Methods in Marine Engineering, MARINE 2017, May (2017).

[16] Ferziger J., Peric M., *Computational methods for fluid dynamics*, Third edition, Springer Verlag, Berlin (2002).

[17] Jasak H., *Error Analysis and Estimation for the Finite Volume Method with Application to Fluid Flows*, PhD Thesis, Imperial College of Science, Technology and Medicine, London (1996).